

## Accepted Manuscript

A computed tomography approach for understanding 3D deformation patterns in complex folds

M<sup>a</sup>José Ramón, Emilio L. Pueyo, Adriana Rodríguez-Pintó, Luis H. Ros, Andrés Pocoví, José Luis Briz, José Carlos Ciria

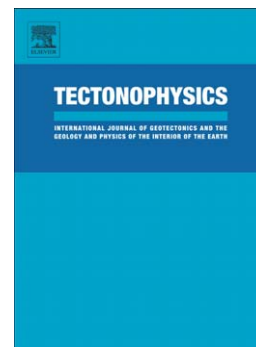
PII: S0040-1951(13)00126-1  
DOI: doi: [10.1016/j.tecto.2013.02.027](https://doi.org/10.1016/j.tecto.2013.02.027)  
Reference: TECTO 125806

To appear in: *Tectonophysics*

Received date: 25 June 2012  
Revised date: 12 February 2013  
Accepted date: 16 February 2013

Please cite this article as: Ramón, M<sup>a</sup>José, Pueyo, Emilio L., Rodríguez-Pintó, Adriana, Ros, Luis H., Pocoví, Andrés, Briz, José Luis, Ciria, José Carlos, A computed tomography approach for understanding 3D deformation patterns in complex folds, *Tectonophysics* (2013), doi: [10.1016/j.tecto.2013.02.027](https://doi.org/10.1016/j.tecto.2013.02.027)

This is a PDF file of an unedited manuscript that has been accepted for publication. As a service to our customers we are providing this early version of the manuscript. The manuscript will undergo copyediting, typesetting, and review of the resulting proof before it is published in its final form. Please note that during the production process errors may be discovered which could affect the content, and all legal disclaimers that apply to the journal pertain.



*A computed tomography approach for understanding 3D deformation  
patterns in complex folds*

M<sup>a</sup>José Ramón<sup>1</sup>; Emilio L. Pueyo<sup>1</sup>; Adriana Rodríguez-Pintó<sup>1,2</sup>;  
Luis H. Ros<sup>3</sup>; Andrés Pocoví<sup>2</sup>; José Luis Briz<sup>4</sup>; José Carlos Ciria<sup>4</sup>

<sup>1</sup>Instituto Geológico y Minero de España (IGME), Zaragoza, Spain

<sup>2</sup>Earth Sciences Department, Zaragoza University, Spain

<sup>3</sup>Radiology Department, Royo Villanova Hospital, Zaragoza, Spain

<sup>4</sup>Computer Science and Engineering Systems Department, Zaragoza University, Spain

**Abstract**

Analog models are an important tool for understanding complexly folded and faulted geological structures. In this paper, we propose the use of X-ray computed tomography to accurately reconstruct the geometry of analog models using an orthogonal reference system and to completely characterize deformation patterns within the modeled structure in 3D. The rheology and radiological contrast of various different materials have been studied showing that EVA sheets are a good choice to model buckling layers. After considering various possibilities to define the reference system, we opted to screen-print two orthogonal sets of parallel lines on the surfaces using minium (lead tetraoxide). The model was then built with gOcad using a series of CT slices that can be closely spaced. This kind of model allows us to reconstruct the volume distribution of strain ellipsoids and can be very accurate and useful to ascertain the orientation of folded lineations in complex structures as well as to characterize the expected deformation on the surfaces. We have built a simple analog model inspired in the Balzes Anticline (located in the External Sierras, Southern Pyrenees) to illustrate the potential of the technique and to analyze the deformation patterns of this complex curved fold that has accommodated significant magnitudes of vertical axis rotation during its formation.

**Keywords**

*Analog models, 3D reconstruction, complex structures, computed tomography,*

*lineations*

## 1. Introduction

Fold-and-thrust belts (FAT belts) tend to be non-cylindrical and non-coaxial in nature, although many research approaches assume the opposite. They have a complex 4D character, usually showing distinctive geometries such as superposed, plunging and conical folds as well as oblique and lateral thrust ramps and folded thrusts. Realistic research needs to be based on a geometric and kinematic framework for these systems that considers these characteristics. For that reason, the geometry and kinematics of oblique structures has been a very active field of research in recent years (see overviews by Wilkerson et al., 2002; Marschak, 2004 and Weil and Sussman, 2004; Yonkee and Weil, 2010).

On the other hand, many kinds of geological simulation (based on paper, cardboard, cloth or plasticine models) have long been performed by geologists to conceptually illustrate and understand complex structures at the laboratory scale. In particular, analog modeling (Hubbert, 1937; Ramberg, 1981) has played an important role in establishing key variables controlling the 3D geometry and kinematics of oblique structures in FTBs (Colletta et al., 1991; Schreurs et al., 2001; Soto et al., 2002 and 2006; Reiter et al., 2011). In addition, X-ray computer tomography (CT), since its development in the 1970s, has been applied in many non-medical fields, among them geology. Specifically, it has been used for understanding the internal 3D geometry of a wide range of earth and planetary materials (see overview by Carlson, 2006). Within this field, the application of CT scanning techniques to reconstruct the 3D geometry of analog models deserves special attention (Colletta et al., 1991; Schreurs et al., 2003; Adam et al., 2008; Harris et al., 2012; Yakymchuk et al., 2012). Reconstructions in 3D of a series of images obtained at different times makes it possible to obtain an overall 4D image. Existing approaches do not, however, enable us to monitor the strain patterns within the model volume during the deformation. Laser scanning and photogrammetry allow the upper surface to be measured in detail (Nilforoushan et al., 2008; Donnadieu et al., 2003; Fischer and Keating, 2005; Leever et al., 2011), but thorough investigation in 3D of internal deformation patterns remains to be achieved.

In this paper, we explore X-ray CT as a method to scan analog models of complex folded structures and to obtain the 3D distribution of strain ellipsoids (as well as any lineation) within the folded volume. We describe how to optimize the selection of materials, CT variables and processing procedures (3D reconstruction). A grid of two parallel sets of lines is drawn on all modeled surfaces to establish a reference system, this being needed to build the model and determine its strain pattern in 3D. We show that these models can be very useful for understanding certain features related to complex settings: 1) folded lineations, 2) the 2D distribution of deformation ellipses on different surfaces within the model, and 3) the 3D distribution of strain tensors in the folded volume. To demonstrate the method, we apply this technique to simulate the Balzes Anticline, a structure from the External Sierras, the frontal fold-and-thrust belt of the Southern Pyrenees. This cover structure can be considered to have a globally preserved volume during its deformation history. Accordingly, it is an appropriate example of complex geometry, namely, a curved anticline that has accommodated important vertical axis rotation during its evolution.

## 2. Methodology

### 2.1. X-Ray CT: principles and settings

X-ray CT is a technique that uses X-rays to obtain cross-section images. The object to be scanned is illuminated with X-rays that interact with electrons, and the contrast in the CT image is generated by local differences in mass density and mean atomic number. Effectively, the intensity in images of slices of the volume scanned is related to the photoelectric absorption property of the material. The sensitivity of CT to material properties like density and composition make it very versatile.

Conventional CT scanners used in medicine usually have millimeter-scale resolution based on using low-energy X-rays (below 125 kV). A scanner with these characteristics is sufficiently powerful for our purpose. If the object scanned has a low radiological density, it is possible to increase the intensity of the emission source. This should, however, be avoided when possible because there is a risk of the gantry (in particular, the X-ray tube) overheating. The proper selection of the materials to build the model is an important factor in achieving clear CT images.

CT has been used before in geology. Specifically, over the past few years CT scanning has been used to quickly obtain repeated 3D images (based on slices) of analog models to explore changes over time (Carlson, 2006). Importantly, X-ray CT allows the 3D visualization of an analog model during an experiment non-invasively and therefore enables both the geometry and its temporal evolution to be studied (providing truly 4D data). It was first applied in the late 1980s and 90s (Colleta et al., 1991) but, due to technical limitations, only a small number of cross-sections were scanned. Current technological improvements have overcome these limitations and allow virtually limitless and closely spaced serial cross-sections to be obtained and processed. Several authors have shown that discrete 3D scanning at different times during an experiment allows 4D analysis of a model (Schreurs et al., 2003; Adam et al., 2008; Harris et al., 2012; Yakymchuk et al., 2012). In this work, we focus on the 3D analysis of complex geometries. The series of X-ray images obtained can be imported into existing software for the 3D reconstruction of geological structures (detailed in Section 2.3 on processing of the data).

We used a *General Electric* HiSpeed FX/i CT scanner at the Royo Villanova Hospital in Zaragoza (Aragon Health Service, SALUD). For the current study, the settings selected to optimize the digital reconstruction were: 1) axial, rather than helical, scans because they generate a sharper image, with a minimum slice thickness of 1 mm; 2) slices spaced 0.5 to 1 cm apart, which is close enough for the resolution required; 3) a high resolution chest CT protocol with a beam energy of 120 kV and low current of 180 mA to avoid the gantry overheating; 4) the lung window to properly view the images on the CT system; and 5) the DICOM format to export the data to the 3D reconstruction software.

## 2.2. Materials and rheology

Cover structures are mainly competent layers folded by buckling (layer-parallel shortening) leading to preservation of volume and areas almost everywhere. However, this principle has to be applied globally as initial volumes may be reduced or increased locally by internal deformation processes (e.g., flexural flow on the limbs and tangential-longitudinal deformation around the hinges; Ramsay, 1977). In this respect,

most types of cloth accomplish one of the basic geometric principles of isometric folding. They can be complexly folded but they will always be (globally) developable in the sense of Lisle (1992). Therefore, simple cloth simulations can be a very useful basis for realistic 3D models.

Among many possible materials, ethylene vinyl acetate sheets (EVA, also known as *expanded rubber* or *foam rubber*) allow isometric folding with some deformation (class 1 folds, Ramsay, 1977), including flexural-flow and flexural-slip as well as tangential-longitudinal strain. It has an amorphous structure, its density can vary widely, from 50 to 200 kg/m<sup>3</sup>, and it has very low water absorption ( $\approx 0.07\%$ ). On the other hand, its tensile strength ranges from 2 to 10 N/cm<sup>2</sup>, while tear strength varies between 2 and 4 N/cm<sup>2</sup>, and it can be elongated by as much as 500%, although common values are around 200-300%. Due to its versatility in industrial applications, it is available commercially in thicknesses covering three orders of magnitude (0.5 to 500 mm), which expands the possibilities of modeling any type of fold geometric setting. The stacking of a given number of EVA sheets (stuck together or free to move) also allows the stratigraphic thickness of the model and the expected mechanism of deformation to be varied. Unlike other materials, EVA has high enough radiological contrast and its boundaries are imaged with sufficient clarity to be accurately redrawn by the image processing software. Alternatively, ethylene propylene diene monomer rubber (EPDM [M-class] rubber) can also be used.

Alternation of different mechanical properties, thicknesses and cohesion between layers produces infinite possibilities and allows modeling of any case under study. Thicknesses of the modeled stratigraphic pile and the wavelength of the folds have to be adapted to the limited size of the CT scanner (usually less than 60 cm in diameter) and the circular geometry of the CT sections has to be taken into account in the model design.

Besides the layer modeling, the reference system characterization is of crucial importance. This reference system is defined with two sets of orthogonal parallel grid lines. We tested many different kinds of materials to simulate the sets of lines: plastic and metallic meshes, strings and cords, and even cloth with linear relief. In most cases, however, there was insufficient radiological contrast, while in the case of metallic lines

the absorption was so high that the radiological image was over-exposed. Moreover, the use of specific layers such as plastic meshes to simulate the set of grid lines has mechanical consequences: 1) it implies detachment from the underlying bed; 2) it does not allow the effect of deformation on the grid lines to be quantified; and 3) the change of the rheology has also consequences for the final geometry. Solid linear elements (cords, strings, wires, etc.) cannot effectively be stuck to an EVA sheet (different mechanical properties) and if they are free to move, they cannot by definition be trusted to provide an accurate reference system. Similarly, the use of cuts or marks in EVA sheets also affects the rheology.

Therefore, to define the reference system we decided to paint a grid on the sheets using highly X-ray absorbing inks, liquids and paints. A wide variety of materials, all of them having high electrical conductivity, were tested for this purpose (Fig. 1A), including graphite, gold and silver inks, aluminum paints, various types of glitter, etc. Of these, minium (red tetraoxide lead) paint was, by far, the most successful material, being found to give a sharp radiological signal without serious streak artifacts in the CT image. Other potentially suitable materials such as graphite, gold, silver and aluminum had too little mass to absorb enough X-ray photons and hence were not detected in the signal or only very faintly. The minium was screen-printed onto the EVA sheets, and this can be done with a good accuracy. Indeed, current screen printing technologies allow computer-aided design of the screen mesh (usually made of nylon and polyester) and mesh sizes up to 0.5 mm. Minium can be used in place of the usual screen printing inks without affecting the performance of the printing process.

The grid that constitutes the reference system (needed to monitor internal deformation in 3D) is made by two orthogonal sets of parallel lines. We explored screen printing the second set of parallel grid lines using a mixture with a different ratio of minium and turpentine or, alternatively, a different quantity of ink. The amount of ink can be varied by changing the line width and an advantage of this approach is that the minium/turpentine mixture for the main and secondary sets of parallel grid lines can be applied at the same time. We found that variation of the line width between 0.5 and 2 mm in the screen worked well. These different amounts of minium produced sufficiently different intensities to allow identification of each set of lines in the CT images (Fig. 1B).

The positioning of the model on the scanner table is also of crucial importance. To clearly identify a line in a CT image it must be perpendicular to the cross-section: the more oblique the greater the scatter; and a line is indistinguishable when it is parallel to the section plane. The ideal orientation is with both sets of grid lines oblique to the cross sections. This is not always possible, however, especially for complex folds with considerable rotation and almost vertical or overturned limbs, a complexity that makes reconstruction more difficult.

### 2.3. Processing of data: reconstruction

Digital Imaging and Communications in Medicine (DICOM, also known as the NEMA Standard PS3<sup>®</sup>) is the standard computer format for handling many different sources of medical images (among them CT). Together with a communication protocol, the file contains a header that provides information concerning the relative position of the different CT sections (location, orientation, spacing, etc.), and this enables us to geo-reference our model. A simple processing based on the data in the header fields (Image Position, Pixel Spacing, Rows and Columns) allows the images to be used like seismic sections in most 3D reconstruction software packages.

Medical software (e.g., *Mimics*<sup>™</sup>) allows processing and editing of 2D image data from CT (and other medical imaging techniques) and it is useful for 3D reconstruction of models. Unfortunately, it was not found to be very effective for the reconstruction of geological models due to the difficulty of accurately identifying important elements such as the different bedding surfaces or the grid lines. For this reason, we decided to use geological software and treat the CT images as geo-referenced cross-section images in gOcad (*Paradigm*) (Fig. 2). The versatile capabilities of gOcad have allowed us to accurately reconstruct the model surfaces and the grid lines over the surface as if the dataset were a series of seismic sections in SEG Y format. Since with CT we can measure closely spaced slices, 3D reconstructions can be highly reliable (much more so than is usually the case for reconstructions based on field data).

The projection or “draping” of an “orthophoto” over the model surface can help further improve the reconstruction, providing in particular accurate data on the position of the

lines. We took an orthophoto using a camera with a 200-mm zoom-lens mount on a tripod. With the help of a laser level, the height of the center of the lens was matched to the center of the model, ensuring that the camera was perfectly perpendicular to the model at a distance of 16 m; this corresponded to an angle of less than  $1^\circ$  between the borders of the model.

In order to double-check the reconstruction, a second technique was used, namely, we digitalized the upper surface by photogrammetry. This is a simple image-based modeling technique that assembles the 3D reconstruction using only photographs taken from different angles. We used *PhotoModeler* ([www.photomodeler.com](http://www.photomodeler.com)) software for this purpose. Photogrammetry has recently been used to check restoration tools (Ramón et al., 2012) and does allow an accurate digital reconstruction of the upper surface though is not valid for the inner surfaces or volume analysis (distribution of strain ellipsoids).

#### 2.4. Post-processing: estimation of strain

A perfectly characterized reference system is key to understanding any folded lineation and to unravel deformation patterns in 2D and 3D. To quantify the deformation, we need accurate measurements of the position of reference points of the structure in the undeformed and deformed states. The fact that this desirable information is unavailable in real cases is what makes analog models all the more important. We reconstruct the model with a tetrahedral mesh formed by the orthogonal set of lines. This reference system is the same in the original and folded states and consequently tracks the deformation. Note that the 3D reference system allows us to predict the orientation of any passive lineation in the folded surface. In addition to this, if we do not have data characterizing the reference system pre-deformation, we must scan the model before as well as after the deformation process to be able to compare the two states.

Thanks to the reference system, we are able to calculate the dilation and the strain ellipsoid for each individual tetrahedron (or triangle in surfaces). Obviously, the spacing of these tensors will be related to the density of our orthogonal reference system. The dilation parameter measures the change of volume (or area in surfaces)  $d=(V_{final}-V_{initial})/V_{initial}$ , while the strain ellipsoid (or ellipse in 2D) measures the anisotropy of

strain and the preferred orientation (stretching lineation). In order to assess the anisotropy of the ellipsoid, we also calculate the ratio between axes ( $P'$ ) and the shape factor ( $T$ ), this ranging between -1 (prolate) and 1 (oblate) and  $T=0$  corresponding to pure triaxial ellipsoids. These parameters (Jelinek, 1981) are regularly used in magnetic fabric analysis and are similar to the axial ratios plotted on a Flinn (1962) diagram ( $L=\text{max/int}$  and  $F=\text{int/min}$ ), although they are much more sensitive to small changes of the ellipsoid since they are based on a logarithmic scale.

The ellipsoid is calculated using the affine transformation matrix  $M$  that relates the points before and after deformation and characterizes the deformation. The matrix coefficients are determined using initial and final tetrahedron vertices. The application of this transformation to a sphere produces an ellipsoid  $A_{\text{ellipsoid}}=(M^{-1})^t \cdot A_{\text{sphere}} \cdot M^{-1}$ . Eigenvalues and eigenvectors of the matrix are the orientation and magnitude of the ellipsoid axes (see the Appendix for further details).

### **3. Case of study: understanding complex structures in 3D**

In this section, we will illustrate the use of CT scanning as a powerful tool to understand complex geometries, expected strain ellipsoids and related folded lineations. Of all the analog models built, scanned and reconstructed we just show here the results from the simulation inspired by the Balzes Anticline, a curved fold located in the easternmost part of the External Sierras (ES) in the Southern Pyrenees. We analyze the orientation of the lineations and the surface and volume deformation of the simulated structure.

#### 3.1. Geological setting

The Balzes Anticline (BA) is an oblique detachment anticline placed on a oblique ramp of the South Pyrenean basal thrust. It is a 17-km long curved structure with a fold hinge trending N011E in the northern sector passing to N152E in the southernmost sector, therefore, in map view, it displays an apparent bending of about 40° (southwestwards convex). The External Sierras represent the southernmost frontal thrust of the west-central part of the Pyrenees. They are characterized by an imbricate thrust system and associated detachment folds developed during Middle Eocene times. The system progressively propagated laterally to the west in more recent times reaching the

Chattian-Aquitania boundary (Puigdefàbregas, 1975; Cámara and Klimowitz, 1985; Millán, 1996; Millán et al., 2000; Muñoz et al., 2013). A second stage of thrusting during Oligocene-Miocene times placed these structures in the hanging wall over the footwall ramp, producing the plunge to the North that affects most of them at the present time (a plunge of about  $13^\circ$  in case of the northern sector of the BA; Figure 3).

The stratigraphy involved in the BA comprises three main marine platform sequences (de Federico, 1981; Barnolas and Teixell, 1994): the Ypresian Alveoline limestones of the first platform outcrop in the core of the structure; the Boltaña Formation (late Ypresian, locally Cuisian) the second platform, represented by  $\approx 300$  m of shallow limestones and siliciclastic input; and the third platform, the Guara Formation, made of up to 650 m of Lutetian limestones. The sedimentation of the Guara Formation was determined by the growing of the Balzes Anticline as attested by an progressive angular unconformity observed in its western flank (Millán et al., 2000; Barnolas and Gil-Peña, 2001). On top of the Lutetian, in the northern part of the anticline, the Sobrarbe deltaic formation (Bartonian) marks the transition to continental conditions, the onset of which is clearly indicated by the thick Campodarbe Group (Puigdefàbregas, 1975) cropping out in the core of the vast Guarga Syncline (Jaca Basin).

Structural and paleomagnetic studies in the area suggest substantial clockwise rotations (CW), related to the westward lateral propagation of the deformation front, which would explain the present-day orientation of the N-S anticlines as well as the reduction of the shortening to the West as deduced from cross section restorations (Puigdefàbregas, 1975; McElroy, 1990; Millán, 1996; Millán et al., 2000; Pueyo et al., 2002; Oliva and Pueyo, 2007; Mochales et al., 2012; Muñoz et al., 2013). CW vertical axis rotations of  $40$  to  $60^\circ$  have been observed in the Boltaña Anticline, to the north of the BA (Mochales et al., 2012 and Muñoz et al., 2013; and references therein), while there are moderate CW rotations of  $15$  to  $20^\circ$  and non-significant rotations in the Bartonian-Priabonian deltaic and continental sediments to the east and south (Sta. Maria de Buil syncline) (Bentham, 1992; Bentham and Burbank, 1996; Pueyo, 2000), pointing to a Bartonian-Priabonian age of the rotational emplacement of the underneath thrust sheets (Mochales et al., 2012).

Recent paleomagnetic investigations of the Balzes Anticline (Rodríguez-Pinto et al.,

2010, 2012 and 2013a&b) have yielded 15 new reliable sites (Fig. 3 and Table 1). Of these, 9 are in the northern portion of the anticline near the villages of Bagüeste (Northwestern flank, 6 sites) and Sarsa de Surta (Northeastern one, 3 sites). There, sampling sites are mostly located in the mudstone facies of the Guara Formation. On the other hand, the six other sites in the Southern sector of the anticline near the San Pelegrin village are mainly in Ypresian and some Lutetian facies: three in the southwest and three in the southeast (Rodríguez-Pintó et al., 2013a&b).

The paleomagnetic record seems to be locked in magnetite and to a lesser extent in sulfides. Apart from some overlapping problems detected in some sites in the Lutetian limestones from the northern sector of the anticline (Rodríguez-Pintó et al., 2013a), which we do not consider here, robust stability tests (fold and reversal) have proven the primary character of the magnetization in the mudstones and Ypresian limestones (Rodríguez-Pintó et al., 2013a&b). We have used the Eocene reference direction (DEC & INC: 004.6°, 53.2°;  $\alpha_{95}$ : 4.6°, k: 9.6) deduced for a central point in the Balzes Anticline (Longitude: 42.31°, Latitude: -0.02° [W]; Rodríguez-Pintó et al., 2012a) to compare to the local vertical-axis rotations.

Mean rotation magnitudes can be estimated for the northern and southern sector of the BA. The former (DEC=55°, INC=42°;  $\alpha_{95}$ =8.8°, k=30.4, N=9 sites) shows a clockwise rotation of 50°, while in the latter the rotation (DEC=28°, INC=37°;  $\alpha_{95}$ =11.4°, k=44.5, N=6 sites) never exceeds 23°. That is, there is a significant difference (27°). A preliminary and simple map-view restoration would allow the northern sector to be restored to a trend similar to the southern one. A simple model is proposed based on paleomagnetic data to explain the rotation of the structure as a secondary bending of the northern part of the fold, while the southern part is only slightly rotated.

### 3.2. Analog model

All information exposed enabled us to perform a simple geometric model of the Balzes Anticline. We do not pretend to perform an exhaustive analysis of the deformation patterns in this anticline but to test the capabilities of the CT scanning in such complex scenario. Our model only considers the overall geometry of the uppermost thrust sheet

(Boltaña-Balzes unit in Figure 3). The analog Balzes model assumes an evaporitic core (Keuper facies) that has been modeled by air in our model (a reasonable assumption considering the rheological contrast with the limestones), the cover rocks (Belsué-Atarés and Campodarbe Formations) on top of the Eocene platform has not been modeled according to the folding ages (they are post-folding). Thus, the top surface of the model represents a first order approximation of the top of the Guara formation and the bottom surface the base of the Ypresian limestones. The geometric scaling of the model has considered some key features: 1) the real variation in the fold axis trend (stereoplots in Figure 3), 2) the wavelength of the anticline ( $\approx 6$  km), 3) the thickness of the modeled stratigraphic pile ( $\approx 300$  m), and 4) the differential vertical axis rotation between the northern and southern sectors ( $27^\circ$ ). The model was designed as a “static” reproduction of the geometry of the anticline (we apply the finite deformation at once, without considering any kinematic constraint) and thus, rheological scaling not been taken into account. The fold was created pushing the northern edge of the model and considering the location of the undeformed foreland (southern edge of the model) that was fixed to the basement of the model (pin-line). Generating this oblique structure based on Balzes Anticline, we see how a secondary fold is formed in the inner part, which could correspond to the Boltaña Anticline southern termination near Paules de Sarsa.

The model was built with two EVA sheets of 58 x 38 x 0.5 cm glued together, giving a total thickness of 1 cm. The EVA sheets were screen-printed with a squared grid of 1 x 1 cm and line widths of 1 and 1.5 mm. One sheet was screen-printed on only one side and the other on both sides, thus we model three surfaces that represent the base, the top and the middle surface of the stratigraphic pile under study. First of all, we scanned the EVA sheets in an undeformed state (horizontal) to set up the reference system. Subsequently, we deformed the sheets following the aforementioned procedure and scanned it again (Fig. 4). We then reconstructed the model from the DICOM cross-sections in gOcad. To double-check the reconstruction from the CT images, we also checked the model against the reconstruction of the upper surface obtained using photogrammetry.

### 3.3. Lineation analysis

As aforementioned, the advantage of these models is that thanks to the reference system we can calculate the orientation of any grid line passively folded. Our primary interest is to understand the 3D patterns of paleomagnetic vectors of complexly folded structures, but, it is worth mentioning that this technique is valid for studying any passive geological lineation like sedimentary structures (paleocurrents), locked stress (slickensides) and strain indicators (mineral stretching), etc...

Here, we compare one set of parallel grid lines of the model with the real paleomagnetic data. The direction of paleomagnetic vectors (their local vertical projection on the model surface) can be seen as a type of lineation (Sellés, 1988; Stewart, 1995; Pueyo et al., 2003) and are unique structural markers that can be clearly established for both the pre- and post-deformation states. In our case, the paleomagnetic data are pre-folding (the stability tests guarantee the primary character of the magnetization) and thus, the model was generated under this evidence. First of all, we need to rotate the entire model to converge to the real axes of the structure. As the orientation of the grid lines in the model was arbitrary and had no inclination, we need to apply a smooth rotation to our "paleomagnetic" record (one of the sets of lines) to converge with the real dataset.

Now, we consider lineation patterns separately in the northern and in the southern flank of the anticline. We select specific sites on the model simulating an outcrop on each side of the anticline. These data are approximately in the same structural location as the real dataset. Inclination has been modeled to fit the real data ( $\approx 40^\circ$ ) rather than the Eocene reference expected in the Pyrenees ( $53^\circ$ ). We project paleomagnetic vectors before and after bedding correction (Fig. 5A). Paleomagnetic data before any correction are clustered in two groups corresponding to the western and eastern limbs of the anticline. As expected, data is grouped after the bedding correction (ABC), and the clustering is better than that seen with the real noisy paleomagnetic data (Fig. 5B).

Given the secondary origin of the fold curvature (that we applied to the model), there is a  $22^\circ$  difference between the mean paleomagnetic direction in the northern and southern sectors, this difference is slightly smaller ( $4^\circ$ ) than detected in the real dataset. These small errors in the lineation, as well as those highlighted by the bedding poles, are not unreasonable. They are likely caused by the analog model, which does not perfectly reproduce the natural geometry. The fold axes of the sectors are similar though again

not exactly equal to those calculated for the real structure. The advantage of the model is its ability to forecast the expected paleomagnetic information on locations that were not sampled in the field.

It is worth underlining that to analyze the uppermost surface we do not need CT imaging and simple photogrammetric techniques could be used alone. In contrast, however, lineation analysis of the internal surfaces will need the CT model as photogrammetry does not provide any information concerning the inside of the structure.

#### 3.4. Surface analysis

Before considering the internal deformation, we analyze the results of the uppermost surface, comparing the results obtained from the reconstruction of the CT images with those from the complementary technique for surface reconstruction: photogrammetry. Our aim with this was to validate the 3D reconstruction based on the CT images. First of all, we compare the distribution of dilation ( $=[\text{Area}_{\text{folded}} - \text{Area}_{\text{restored}}] / \text{Area}_{\text{restored}}$ ) across the entire surface. The photogrammetric technique is more accurate for the upper surface reconstruction and gives clearer results but they are equivalent in meaning (Fig. 6A). This is basically due to the greater accuracy of the photogrammetric method in reconstructing the exact location of the nodes (intersections between the two sets of lines).

If we now analyze all the three surfaces derived from the CT modeling (Fig. 6B), we observe tangential-longitudinal strain in line with Ramsay (1977) and Gairola (1978), extension in the anticlines outer hinges of the upper surface (positive dilation), conservation of area in the middle neutral surface and compression (negative dilation) of the inner hinges in the lower one. We observe consistent senses of dilation in the synclines: positive on the outer arc and negative on the inner one. It is worth noticing that the areas with clear dilation are significantly different at the two surfaces (upper and lower): in the lower surface the maximum dilation is concentrated in a much smaller area and is more intense than in the upper one. This observation fully agrees with the expected differences in arc lengths between outer and inner hinges.

The most deformed areas are precisely the ones of maximum mean curvature (mean between the two principal normal curvatures:  $M=(k1+k2)/2$ ). Since we are unable to derive the anisotropy from the curvature, we plot the strain ellipses in terms of the ratio of the axes and the orientation of the main axis. In the CT model, the areas of higher anisotropy (ratio between major and minor axis) correspond with areas of compression: the syncline between Balzes and Boltaña anticline in the upper surface (synclastic synform according to Lisle and Toimil, 2007) and both anticlines in the lower surface (synclastic antiform). This observation is in agreement with the distribution of dilation across the upper and lower surfaces. As suggested above, this may be caused by the concentration of deformation in the inner-arc zones, which have to accommodate an equal amount of volume change in a smaller deformed volume. On the other hand, the Gaussian curvature ( $G=k1\cdot k2$ ; Gauss, 1827) is concentrated in the area of superposed folding (Boltaña-Balzes) and there are no significant differences between the three surfaces.

The strain ellipse gives us extra information about anisotropy. As observed before, upper and lower surfaces display opposite results. The same applies for the orientation patterns. The directions of the major axis of the ellipse are perpendicular for upper and lower surfaces. In the middle (neutral) surface there is no clear preferential orientation of deformation (and, in any case, the magnitude is very small). Focusing on the upper surface, we observe that the main axis orientation is perpendicular to the fold axis in both anticlines (Boltaña and Balzes) and parallel to the fold axis in the middle syncline. On the other hand, for the lower surface, the main axes of the ellipses follow the fold axis orientation, being located in the inner part of the anticline.

### 3.5. Volume analysis

The volume analysis is carried out for the upper and lower volumes separately (Figs. 7 and 8). The main problem of the model is the low strain ratio (major axis/minor), caused by the small ratio between the modeled thickness and the fold wavelength.

The low anisotropy (mostly less than 2) is attested by the P' vs. T diagram (Jelinek, 1981). To explore the deformation, we decided to use these magnetic fabric parameters since they are more sensitive to small variations in the tensor geometry than the simple

axial ratio (i.e., Flinn diagram, 1962). Here,  $P'$  is proportional to the strain ratio of the ellipsoid and  $T$  ranges between 1 (pure oblate) and -1 (pure prolate). In this graph (Fig. 7A), the points are widely scattered reflecting the low strain ratio of the ellipsoid. Similar evidence is obtained from the mean normal curvature vs. dilation diagram (Fig. 7A). Apart from the narrow ranges of variation (-0.03 to 0.03 and -0.6 to 0.6 respectively), most of the data fall close to the origin (non-deformation zone), although some data points on the upper surface with negative dilations spread towards negative curvatures (synclinal hinges), and some points on the lower surface with negative dilations tend to positive curvatures (anticlinal hinges).

Due to the considerable noise caused by the low anisotropy and the large number of tensors, we tried classifying the data according to some simple variables (Fig. 7B). First, mean curvature ( $M$ ) readily allows localization of the hinges, both anticlines (positive values) and synclines (negative ones). Second, the bedding dip constrains the boundary between flanks and hinges. Dips  $< 30^\circ$  can be unambiguously classified as fold hinges. Finally, small dips ( $< 30^\circ$ ) and low curvature values ( $< |10|$ ) represent the flat and undeformed portions of the model. Therefore a clear distinction can be established between all these model zones (besides the classification of Lisle and Toimil [2007] that also considers the Gaussian curvature).

The mean curvature allows a quick (and coarse) segregation of anticlines and synclines hinges. The distribution of the shape of the ellipsoid ( $T$ ) is very noisy (Fig. 7C) when we plot all the data together. If, however, we concentrate only on the hinges (flat and flanks zones are not considered) some patterns can be seen: curvature varies over a narrower range (between 10 and 20) in the anticlines than in the synclines (between -10 to -30). This must be related to the relatively large non-coaxial deformation in the curved syncline (Fig. 7B), compared to in the anticline, which corresponds to the minimum Gaussian curvature. The volume tensors seem to be slightly more oblate, and this could be related to the tangential-longitudinal deformation in hinge zones.

Despite the generally low anisotropy (strain ratio), this parameter is related to map view location (Fig. 7D). Selecting the ellipsoids with  $P' > 1.5$ , we can see that they tend to be localized in specific zones, namely, the fold hinges. Consistent with the model design (the sheets were fixed), most deformation has been accommodated in the hinges and

very little in the flanks (tangential-longitudinal strain). Further, there is more deformation in the northern sector (relatively closely spaced points with  $P' > 1.5$ ) than the southern one (more scattered points). Finally, we plotted on the map the shape of the tensor (T) of the hinge zones alone (only those with significant anisotropies:  $P' > 1.3$ ). Despite the remaining noise, oblate ellipsoids seem to be localized in the outer hinges (Balzes anticline and the curved syncline).

Interesting results to understand the distribution of deformation across the model can be also derived from exploring key variables in map view. This example in Figure 8 shows a general compression of the structure especially in the inner arc of the synclastic antiform (lower volume). The expected preservation of volume is not completely respected because there is no clear extension in the upper volume. This can be attributed, according to the surface analysis, to the values of compression in the lower surface (inner arc) being higher than those of extension in the upper surface (outer arc). Moreover, deformation is concentrated in a smaller volume in the lower sheet than the upper one. As observed before, the normalized anisotropy ( $P'$  parameter  $\approx$  strain ratio) is higher in areas of compression where more deformation is concentrated in less space (again where the maximum Gaussian curvature in absolute value is located). This is consistent with the surface analysis: the anticline hinge anisotropy seems to be smaller and more diffuse in the upper volume than in the lower one.

Since anisotropy is quite small (close to 1) there is no clear shape factor distribution. Nevertheless, strongly oblate ellipsoids<sup>1</sup> tend to concentrate in the anticline. We could expect to find oblate ellipsoids in the upper volume and prolate ellipsoids in the lower volume but in this case layers are not thick enough for that pattern to be observed. The orientation of the minor axis is, however, coherent with the expected values: vertical in the upper volume and horizontal in the lower volume. The major axis is not that clear because it is very similar to the intermediate axis in oblate ellipsoids.

In future models, use of greater thicknesses will help to produce larger anisotropies in tangential-longitudinal strain folds for an equivalent wavelength. This can be expected to strengthen the results, confirming the usefulness of the models to predict any

---

<sup>1</sup>  $T \approx 1$ , major axis  $\approx$  intermediate  $>$  minor

deformation pattern and to double-check restoration results.

#### 4. Conclusions

In this paper, we show that CT scanning of analog models is a powerful tool for exploring and understanding complexly folded structures in 3D. Deformation mechanisms can be reproduced depending on the scaling and the rheology of the materials used in the model, and the model resolution can be adapted as required by changing the density of an orthogonal reference system.

Sheets of EVA were selected to build the analog models because this material gives enough radiological contrast and presents an appropriate rheology to simulate active folds. The screen-printing of lines with different thicknesses of minium paint allows a suitable orthogonal reference system to be set up. The model is built from a series of CT slices treated as seismic sections using geological software (gOcad). Deformation is quantified with the calculation of dilation as change of volume (or area in 2D) and the strain ellipsoid to assess anisotropy.

The model is well known in both the pre- and post-deformation states because the initial and final volume, areas and lengths are monitored in detail. Given this, CT scanning of analog models is a useful tool:

- 1) To calculate the expected orientation of any linear element, being particularly interesting for understanding paleomagnetic vectors
- 2) To determine deformation patterns of surfaces
- 3) To obtain the distribution of the strain tensors in 3D.

We have produced an idealistic simple model of a complex anticline to test the capabilities of the method. The model was inspired in the Balzes Anticline, a curved and non-coaxial fold from the Southern Pyrenees. We successfully compared one of the set of parallel grid lines of the model with real paleomagnetic data in the northern and southern portions of the anticline. The deformation analysis identifies dilation of opposite senses in upper and lower surfaces, with higher magnitudes in areas of compression. Surface anisotropy reflects a perpendicular orientation of the main axis with respect to the fold axis in the anticlines. Volume anisotropy is smaller, although it

is possible to distinguish horizontal ellipsoids in the upper volume and vertical ones in the lower one.

Further, CT scan models have additional applications. They can be used to check the reliability of automatic reconstruction methods and programs because they can be designed to achieve a high level of accuracy (e.g., by closely spacing the radiological slices). They can also be used to leverage partial or biased information, but in this case the geometrical and geomechanical properties must be properly scaled to identify the materials, model stratigraphic volumes and reproduce the mechanical properties of rocks. In the same way, CT scan models also allow the validity of any 3D restoration methods and software to be checked since the geometry and kinematics of the model is perfectly known and the geometry of the undeformed state is also fixed. Finally, the techniques proposed in this paper could also be adapted and applied to sandbox and centrifuge analog models to monitor the strain pattern in 4D.

***Acknowledgements:** Research funding came from grants for the Pmag3Drest (CGL-2006-2289-BTE, CGL2009-14214) and Geokin3D-Pyr (CTPP01/2007-INTERREGIIIb-EU) projects. MJRO has a contract as a technical scientific officer (PTA2007-0282). We are grateful for technical assistance from the Radiology Service of the “Royo Villanova” Hospital (Aragon Health Service) as well as from the Image analysis group at the University of Zaragoza. Gelu López helped with the building of some of the models. Lastly, we also thank Alberto Carrion and Juanjo Villalaín for advice on issues related to physics and to the radiological technology used in this project.*

## References

- Adam, J., Schreurs, G., Klinkmüller, M., Wieneke, 2008. 2D/3D Strain localization and fault simulation in analogue experiments: insights from X-ray computed tomography and tomographic image correlation. *Boll. di Geofisica*, 49, 21-22.
- Barnolas, A. and I. Gil Peña. 2001. Estructura secuencial del relleno sedimentario de la Cuenca de antepaís surpirenaica y su relación con la evolución del orógeno. *Geotemas*, vol. 2, pág. 37-41.
- Barnolas, A. and A. Teixell. 1994. Platform sedimentation and collapse in a carbonate-dominated margin of a foreland basin (Jaca basin, Eocene, southern Pyrenees). *Geology* (ISSN: 0091-7613), 22, 1107-1110.
- Barnolas, A., Samsó J. M., Malagón, J., Gil-Peña, I., Montes, M., Rico, M., (in press). Mapa geológico y memoria de la Hoja nº 249, Alquezar, del Mapa Geológico de España a escala 1:50.000 (MAGNA). Instituto Geológico y Minero de España, Madrid.
- Bentham, P. A., 1992. The tectono-stratigraphic development of the western oblique ramp of the south-central Pyrenean thrust system, Northern Spain. Ph.D. thesis, University of Southern California.

253pp.

- Bentham, P and D. W. Burbank, 1996. Chronology of Eocene foreland basin evolution along the western oblique margin of the South-Central Pyrenees. In: Tertiary basins of Spain. Edit: Friend, P.F., Dabrio, C.J. Cambridge Univ. Press, pp. 144-152.
- Cámara, P. and J. Klimowitz, 1985. Interpretación geodinámica de la vertiente centro-occidental surpirenaica (Cuencas de Jaca-Tremp). *Estudios geológicos*, 41, 391–404.
- Carlson, W. D., 2006. Three-dimensional imaging of earth and planetary materials. *Earth and Planetary Science Letters* 249, 133–147.
- Colletta, B., Letouzey, J., Pinedo, R., Ballard, J. F., Balé, P., 1991. Computerized X-ray tomography analysis of sandbox models: Examples of thin-skinned thrust systems. *Geology*; v. 19; no. 11; p. 1063-1067.
- De Federico, A., 1981. La sedimentación de talud en el sector occidental de la cuenca paleógena de Aínsa. *Publ. de Geología, University of Barcelona*, 12. 271 pp.
- Donnadieu, F., Kelfoun, K., van Wyk de Vries, B., Cecchi, E., Merle, O., 2003. Digital photogrammetry as a tool in analogue modelling: applications to volcano instability. *Journal of Volcanology and Geothermal Research* 123; 161-180.
- Fischer, M. P., Keating, D. P., 2005. Photogrammetric techniques for analyzing displacement, strain, and structural geometry in physical models: Application to the growth of monoclinial basement uplifts. *Geological Society of America Bulletin* 2005; 117, no. 3-4;369-382.
- Flinn, D. 1962. On folding during three-dimensional progressive deformation. *Geol. Soc. London Quaterly Journal*, v. 118, pp 385-433.
- Gairola, V. K., 1978. Strain distribution across an experimental single-layer fold. *Tectonophysics* 44, 27-40.
- Gauss, C. F., 1827. *Disquisitiones circa generales superficies curvas*. First published in *Commentationes societatis regiae scientiarum Gottingensis recentiores*, vol. VI, 1828. 12 sections, 224 pp.
- Harris, L.B.; Yakymchuk, C.; Godin, L., 2012. Implications of centrifuge simulations of channel flow for opening out or destruction of folds. *Tectonophysics* 526–529, 67–87
- Hubbert, M. K., 1937. Theory of scale models as applied to the study of geologic structures. *Geol. Soc. Amer. Bull.*, 48, 1459-1520.
- Jelinek, V., 1981. Characterization of the magnetic fabric of rocks. *Tectonophysics*, 79, 63–67.
- Leever, L., Gabrielsen, R., Sokoutis, D., Willingshofer, E., 2011. The effect of convergence angle on the kinematic evolution of strain partitioning in transpressional brittle wedges. Insight from analog modeling and high-resolution digital image analysis. *Tectonics*, v.30, p.1-25, TC2013, doi:2010TC002823.
- Lisle, R., 1992. Constant bed-length folding: three-dimensional geometrical implications. *Journal of Structural Geology*, 14 (2), 245-252.
- Lisle, R. J. and Toimil, N. (2007). Defining folds on three-dimensional surfaces. *Geology* 35 (6), 519-522.
- Marshak, S., 2004. Salients, recesses, arcs, oroclines, and syntaxes; a review of ideas concerning the formation of map-view curves in fold-thrust belts. In: *Thrust tectonics and hydrocarbon systems*.

- Edited by: McClay, Ken R. AAPG Memoir, vol.82, pp.131-156, 2004
- McElroy, R., 1990. Thrust kinematics and syntectonic sedimentation: the Pyrenean frontal ramp, Huesca, Spain. Unpublished Ph.D. thesis, University of Cambridge, p. 175.
- Millán, H., 1996. Estructura y cinemática del frente de cabalgamiento surpirenaico en las Sierras Exteriores Aragonesas. Tesis Doctoral Universidad de Zaragoza, p. 330. Published in 2006 in: Colección de Estudios Altoaragoneses, vol. 53. Instituto de Estudios Altoaragoneses, Huesca, ISBN 84-8127-165-9, 398 pp.
- Millán, H., Pueyo, E. L., Aurell, M., Luzón, A., Oliva, B., Martínez-Peña, M. B. and Pocoví, A., 2000. Actividad tectónica registrada en los depósitos terciarios del frente meridional del Pirineo central. *Rev. Soc. Geol. España* 13(2), 279-300.
- Mochales, T., Casas, A. M., Pueyo, E. L., Barnolas, A., 2012. Rotational velocity for oblique structures (Boltaña anticline, southern Pyrenees). *Journal of Structural Geology* 35, 2-16. doi:10.1016/j.jsg.2011.11.009
- Muñoz, J.A.; Beamud, B.; Fernández, O.; Arbués, P.; Dinarès-Turell, J.; Poblet, J. (2013 in review). The Ainsa Fold and Thrust Oblique Zone of the Central Pyrenees: Kinematics of a Curved Contractional System from Paleomagnetic and Structural Data. *Tectonics*
- Nilforoushan, F., Koyi, H., Swantesson, J. O. H., Talbot, C. J., 2008. Effect of basal friction on surface and volumetric strain in models of convergent settings measured by a laser scanner. *Journal of Structural Geology* 30, 366–379.
- Oliva-Urcia, B.; Pueyo, E. L. (2007). Gradient of shortening and vertical-axis rotations in the southwestern Pyrenees (Spain). *Revista de la Sociedad Geológica de España*, 20 (2) 105 -118.
- Pueyo, E. L., 2000. Rotaciones paleomagnéticas en sistemas de pliegues y cabalgamientos. Tipos, causas, significado y aplicaciones (ejemplos del Pirineo Aragonés). Ph.D. thesis, Universidad de Zaragoza. 296 pp.
- Pueyo, E. L., Millán, H., Pocoví, A., 2002. Rotation velocity of a thrust: a paleomagnetic study in the External Sierras (Southern Pyrenees). *Sedimentary Geology*, 146, 191 – 208.
- Pueyo, E. L., Parés, J. M., Millán, H., Pocoví, A., 2003. Conical folds and apparent rotations in paleomagnetism (A case studied in the Southern Pyrenees). In: *Paleomagnetism applied to tectonics; a tribute to Rob Van der Voo*. Edited by: Mac Niocaill, C.; Torsvik, T. H.; van der Pluijm, B. A. *Tectonophysics* 362 (1-4) ( 345-366).
- Puigdefábregas, C., 1975. La sedimentación molásica en la cuenca de Jaca. *Pirineos* 104, 1e188.
- Ramberg, H. 1981. Gravity, Deformation, and the Earth's Crust in Theory, Experiments and Geological Applications. 2nd Edition Academic-Press, London, New York.
- Ramón, M. J, Pueyo, E. L, Briz, J. L., Pocoví, A., Ciria, J. C., 2012. Flexural unfolding using paleomagnetic vectors. *Journal of Structural Geology* 35, 28-39.
- Ramsay J.G., 1977. Plegamiento y fracturación de las rocas. Hermann Blume, pp. 361-390.
- Reiter K., Kukowski N., Ratschbacher L., 2011. The interaction of two indenters in analogue experiments and implications for curved fold-and-thrust belts. *Earth and Planetary Science Letters* 302 (1-2) 132-146.
- Rodríguez-Pintó, A., Pueyo, E. L., Pocoví, A., Barnolas, A., 2010. Paleomagnetic analysis in the Balzez

- anticline (Southern Pyrenees); Vertical-axis rotations and kinematic implications. *Trabajos de Geología*, 30 (1) 169 – 175.
- Rodríguez-Pintó, A., Pueyo, E. L., Barnolas, A., Samsó, J. M., Pocoví, A., Gil-Peña, I., Mochales, T., Serra-Kiel, J., 2012 Lutetian magnetostratigraphy in the Santa Marina section (Balzes anticline, Southwestern Pyrenees). *Geotemas* 13, 1184-1187.
- Rodríguez-Pintó, A.; Pueyo, E. L.; Pocoví, A.; Ramón, M. J.; Oliva-Urcia, B. (2013a) Structural control on overlapped paleomagnetic vectors: A case study in the Balzes anticline (Southern Pyrenees). *Physics of the Earth and Planetary Interiors*, 215, 43–57. doi: 10.1016/j.pepi.2012.10.005
- Rodríguez-Pintó, A.; Pueyo, E.L.; Serra-Kiel, J.; Barnolas, A.; Samsó, J. M.; Pocoví, A. (2013b). The Upper Ypresian-Lutetian in the San Pelegrín section (Southwestern Pyrenean Basin): magnetostratigraphy and larger foraminifera correlation. *Palaeogeography, Palaeoclimatology, Palaeoecology* 370, 13–29. doi: 10.1016/j.palaeo.2012.10.029
- Schreurs, G., Hanni, R., Vock, P., 2001. 4-D Analysis of analog models: experiments on transfer zones in fold-and-thrust belts. In: Koyi, H.A. & Mancktelow, N.S. (eds) *Tectonic Modeling. A Volume in Honor of Hans Ramberg*. Geological Society of America Memoir, 193, 179-190.
- Schreurs, G., Hänni, R., Panien, M., Vock, P., 2003. The analysis of analogue model experiments by helical X-ray computed tomography. In: Mees, F., Swennen, R., Van Geet, M. and Jacobs, P. (eds). *Applications of X-ray computed tomography in the geosciences*. Geological Society London, Special Publications, 215, 213-223.
- Sellés-Martínez, J., 1988. Las correcciones estructural y tectónica en el tratamiento de los datos magnéticos. *Geofísica Internacional*, 27-3, 379-393 pp.
- Stewart, S. A., 1995. Paleomagnetic analysis of plunging fold structures: Errors and a simple fold test, *Earth Planetary Science Letters*, 130, 57-67 pp.
- Soto, R., Casas, A. M., Storti, F., Faccenna, C., 2002. Role of lateral thickness variations on the development of oblique structures at the western end of the South Pyrenean Central Unit. *Tectonophysics* 350(3), 215-235.
- Soto, R., Casas-Sainz, A. M., Pueyo, E. L., 2006. Along-strike variation of orogenic wedges associated with vertical axis rotations. *Journal of Geophysical Research (Solid Earth)*, 111 (B10), B10402-B10423.
- Weil, A.B. and Sussman, A. J., 2004. Classification of curved orogens based on the timing relationships between structural development and vertical-axis rotations, in *Orogenic Curvature: Integrating Paleomagnetic and Structural Analyses*, edited by A. J. Sussman and A. B. Weil, *Spec. Pap. Geol. Soc. Am.*, 383, 1–17.
- Wilkerson, M. S., Apotria, T., Farid, T., 2002. Interpreting the geologic map expression of contractional fault-related fold terminations; lateral/oblique ramps versus displacement gradients. *Journal of Structural Geology*, vol.24, no.4, pp.593-607.
- Yakymchuk, C.; Harris, L.B.; Godin, L., 2012. Centrifuge modelling of deformation of a multi-layered sequence over a ductile substrate: 1. Style and 4D geometry of active cover folds during layer-parallel shortening. *Int J Earth Sci (Geol Rundsch)* 101:463–482
- Yonkee, A.; Weil, A.B., 2010. Quantifying vertical axis rotation in curved orogens: Correlating multiple

data sets with a refined weighted least squares strike test. *Tectonics*, 29, TC3012

ACCEPTED MANUSCRIPT

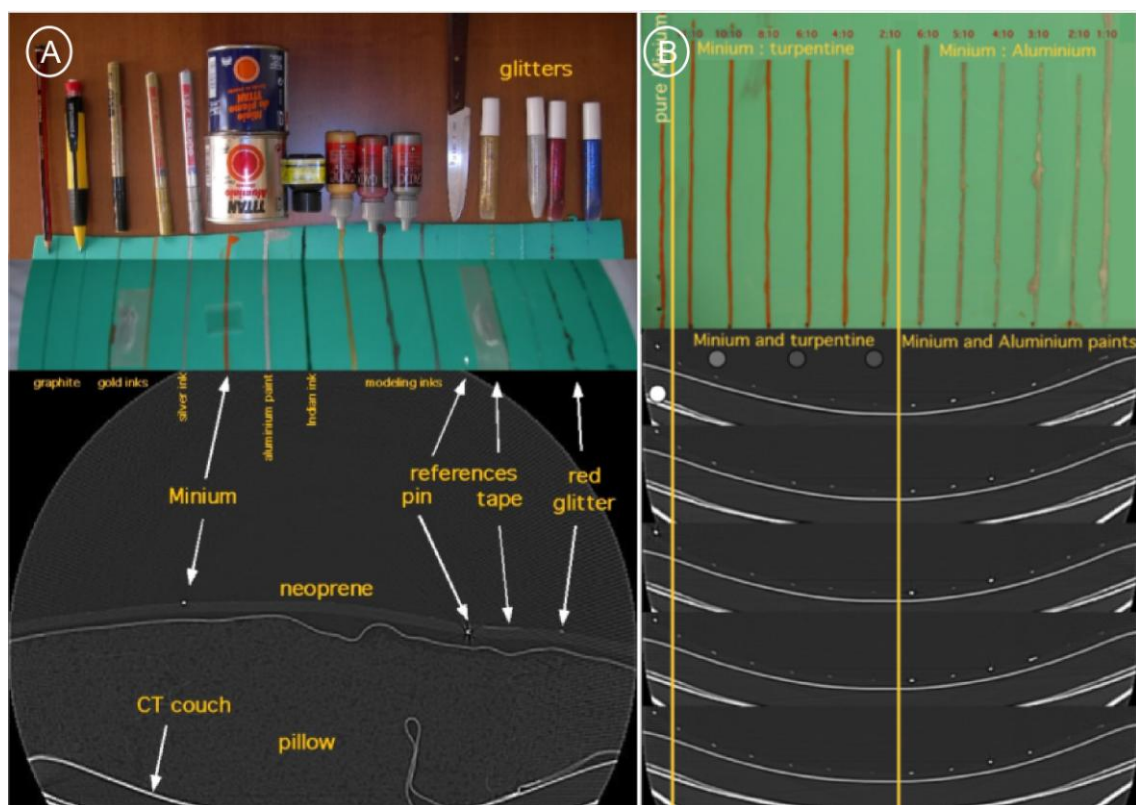
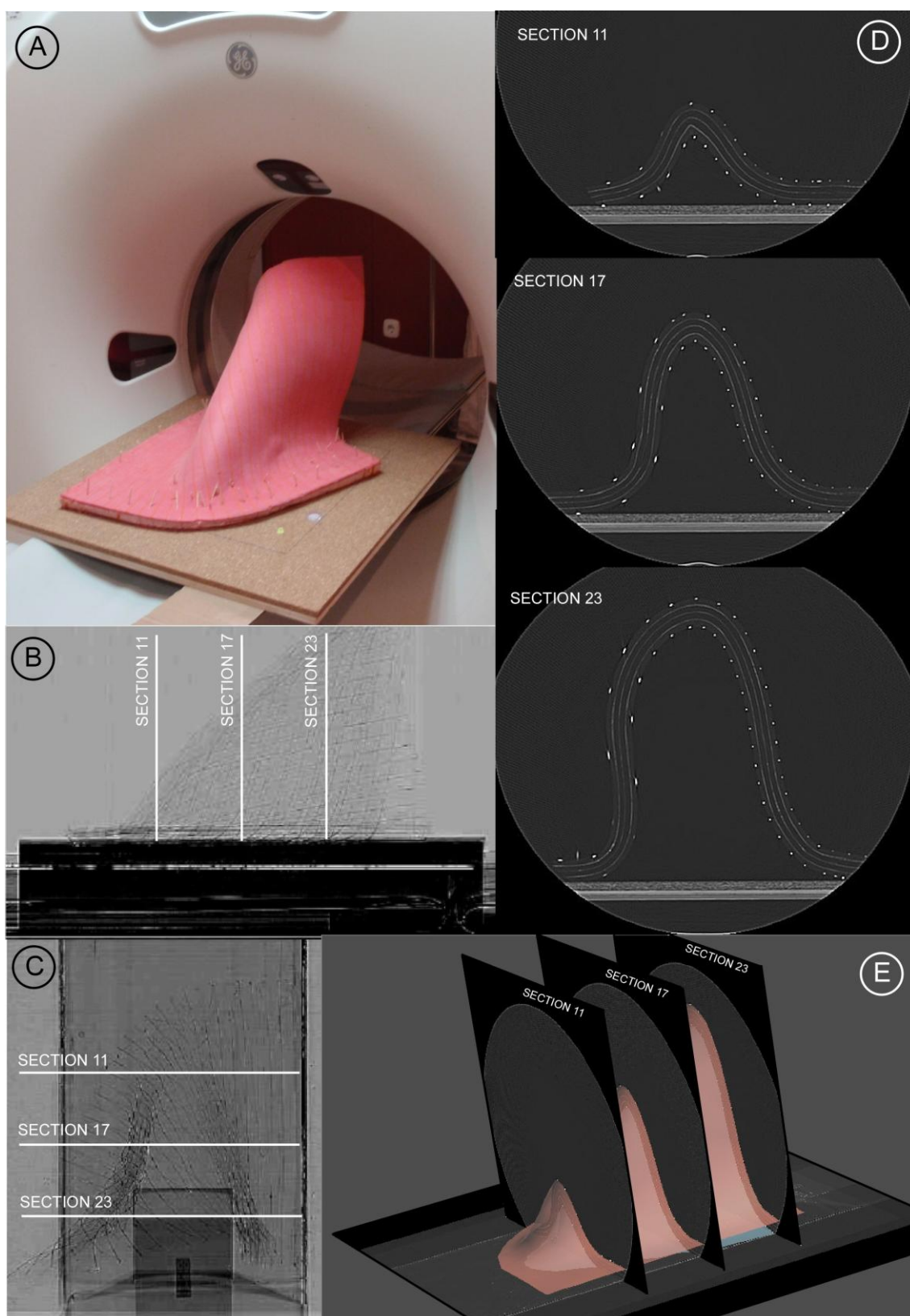


Fig. 1

**Fig. 2**

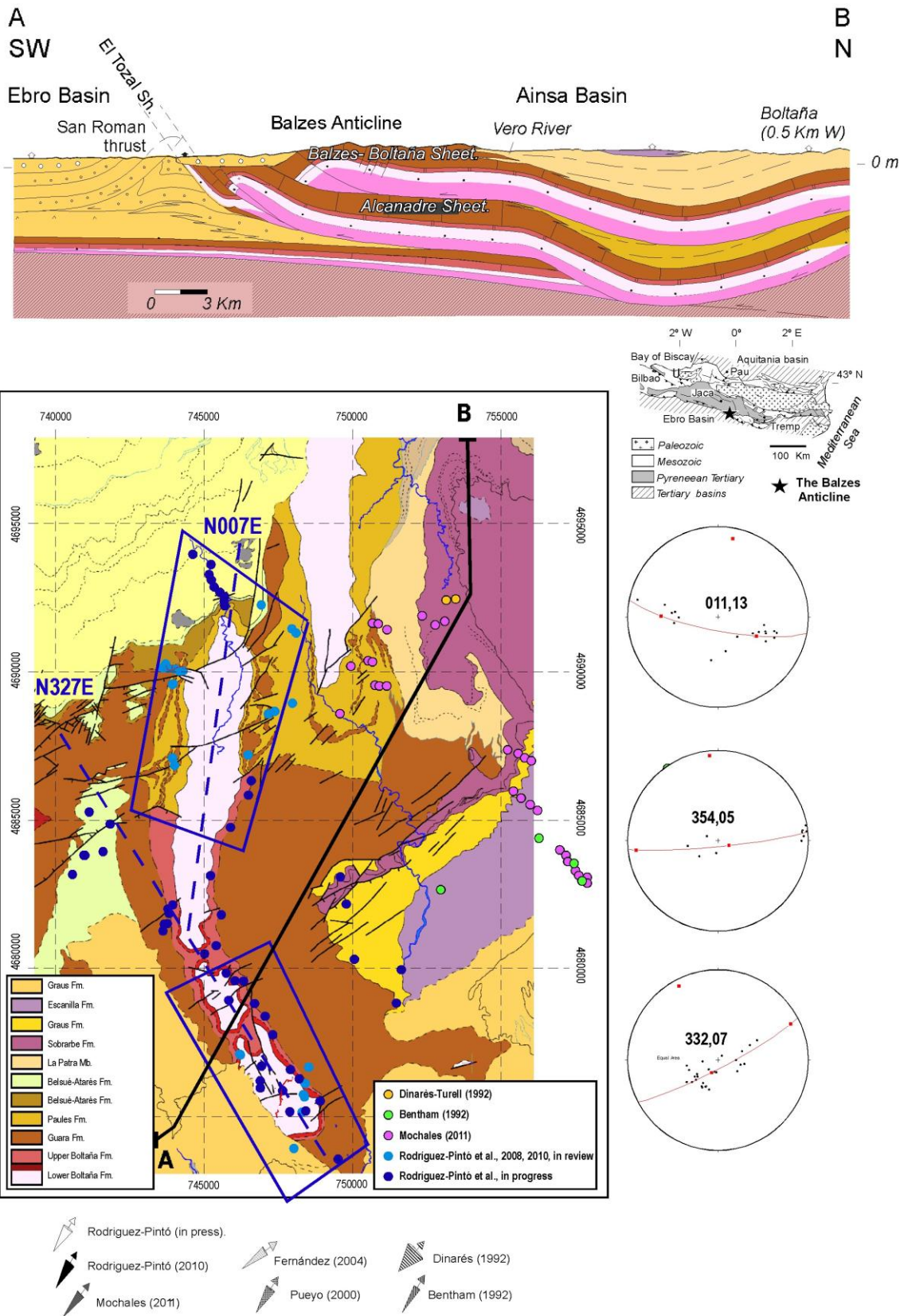


Fig. 3

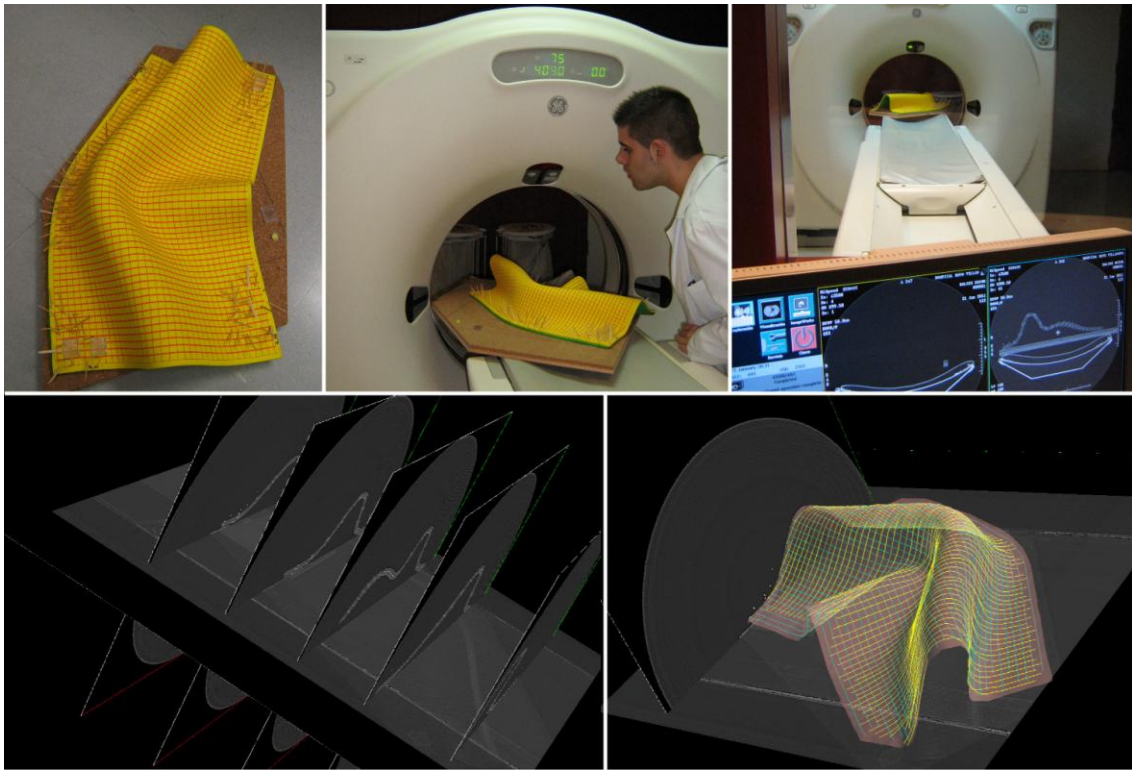


Fig. 4

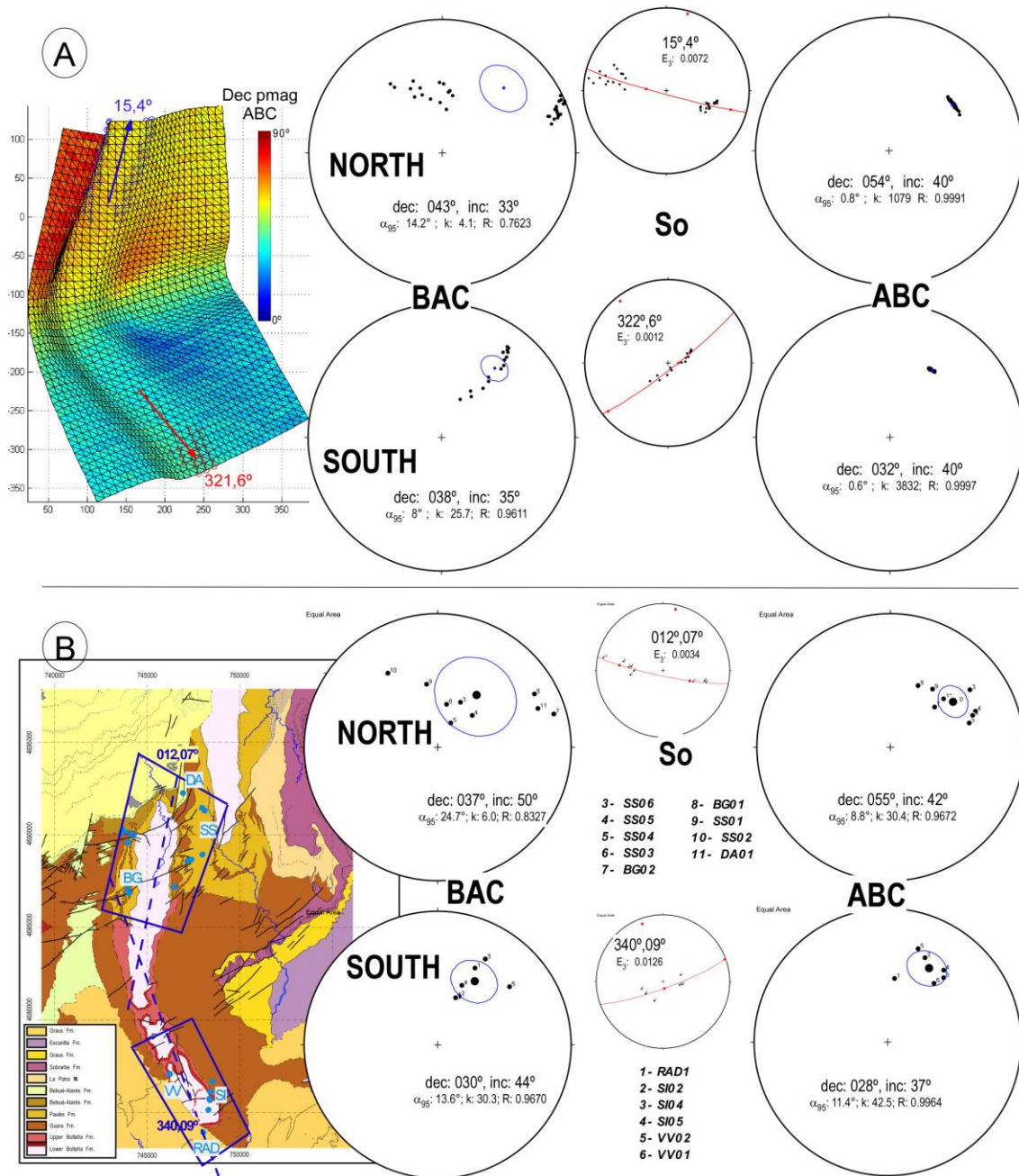


Fig. 5

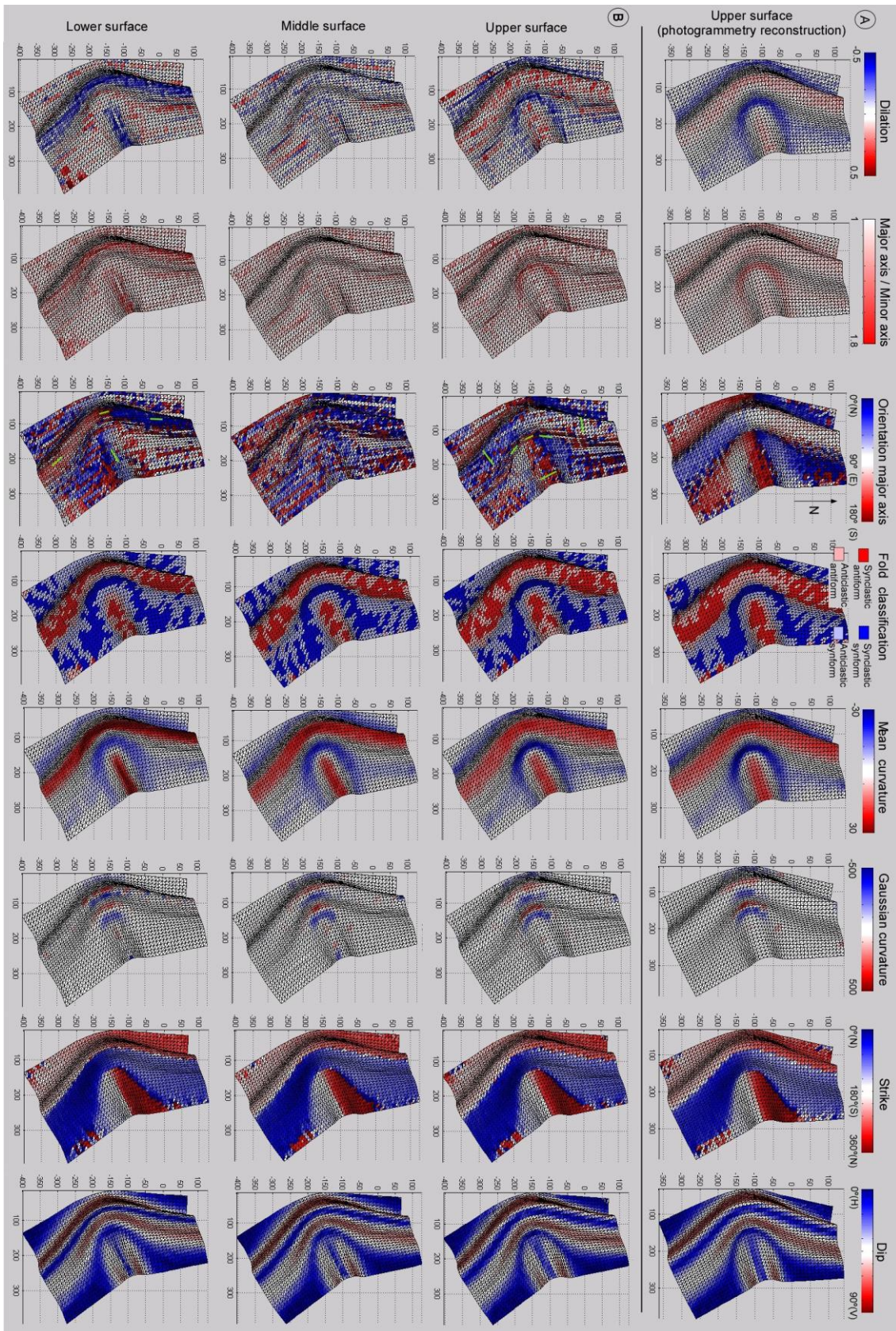


Fig. 6

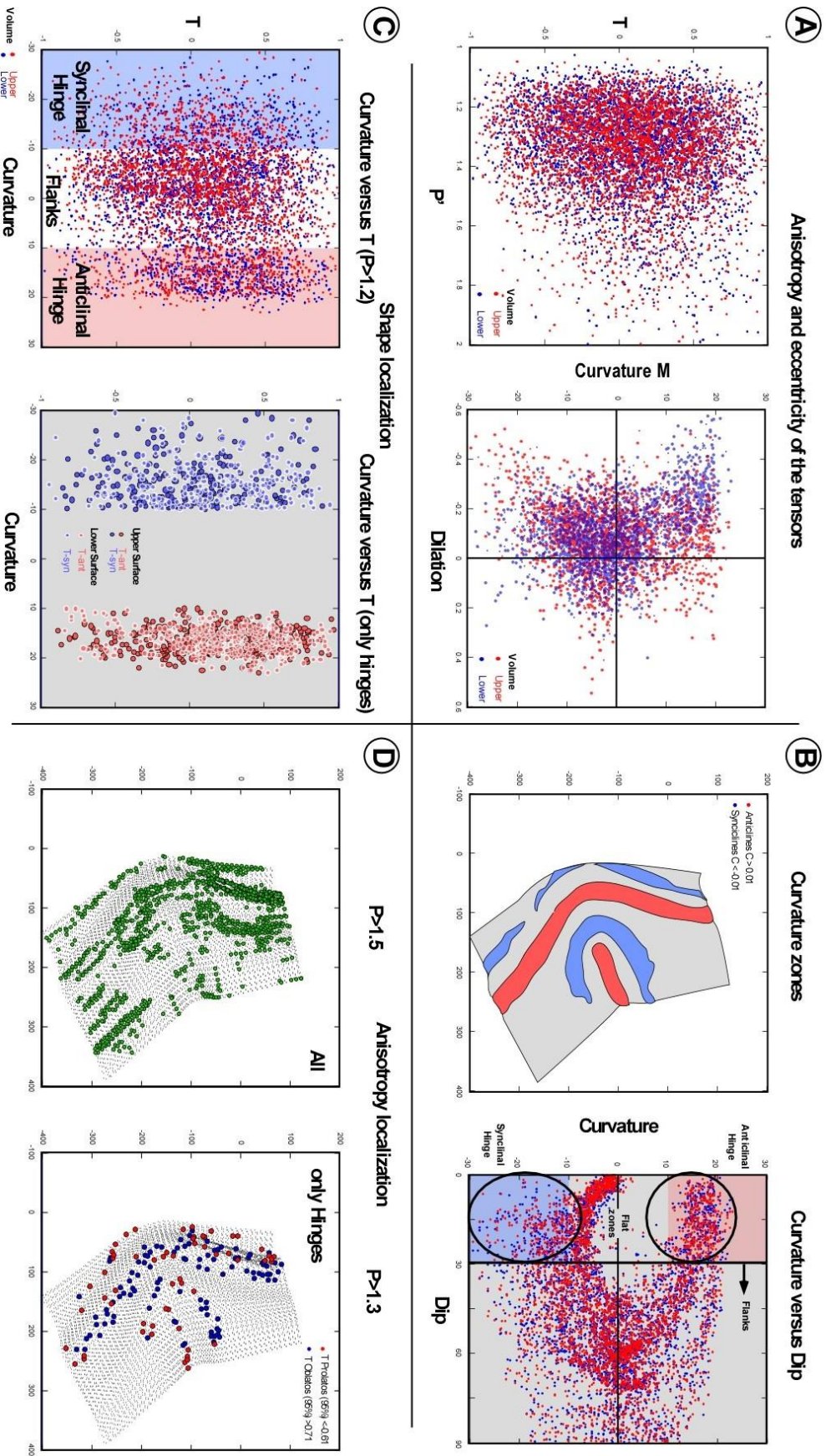


Fig. 7

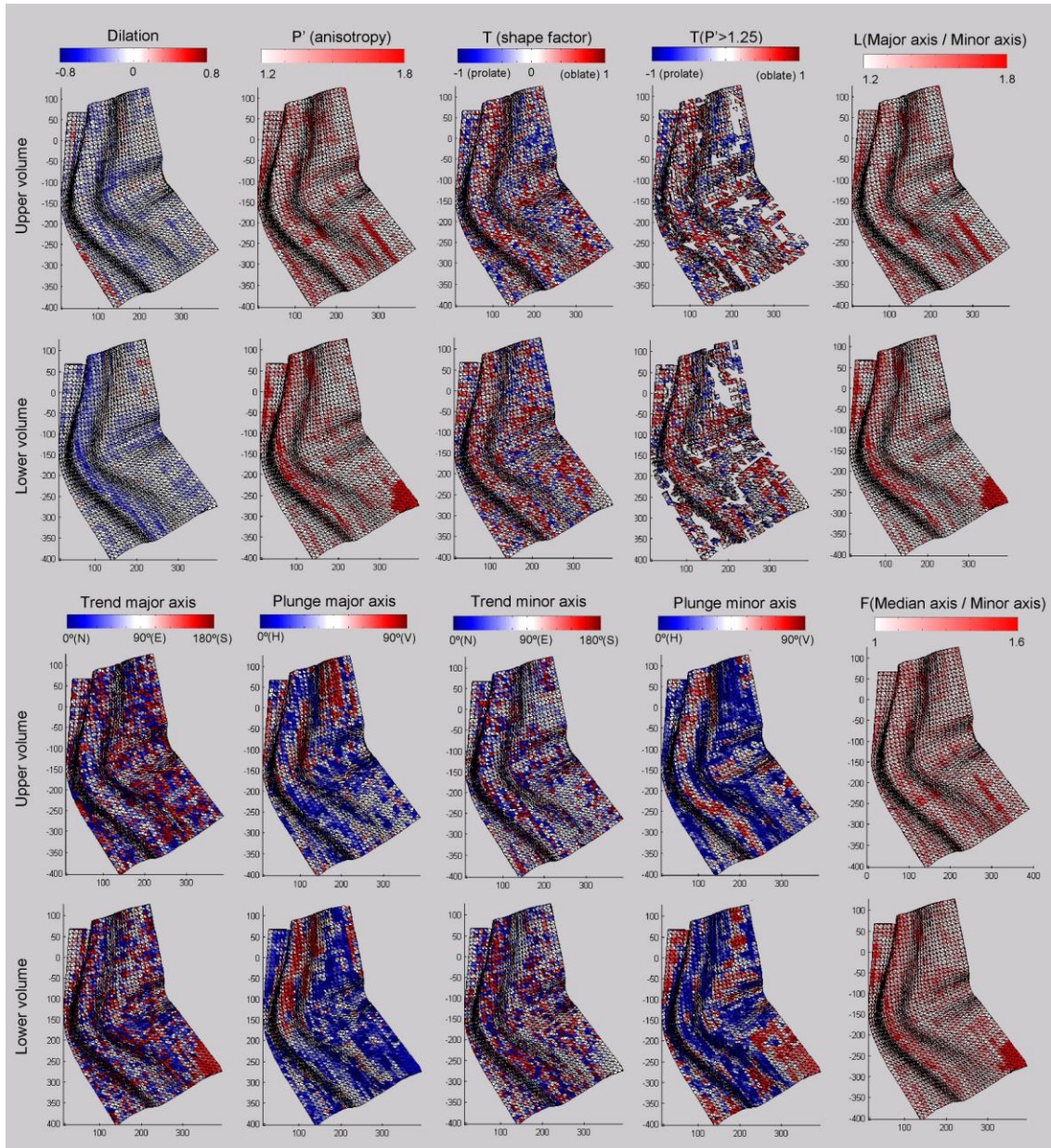
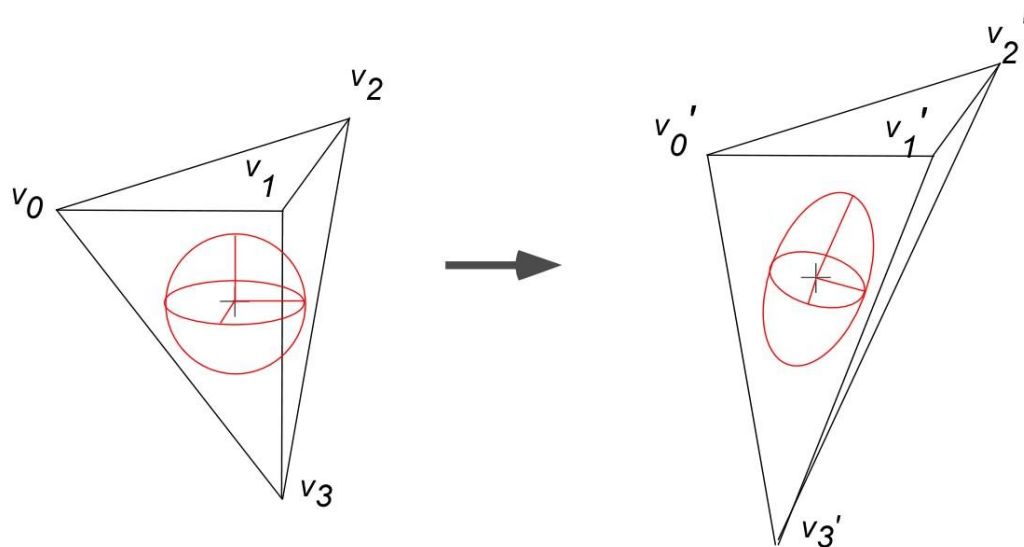
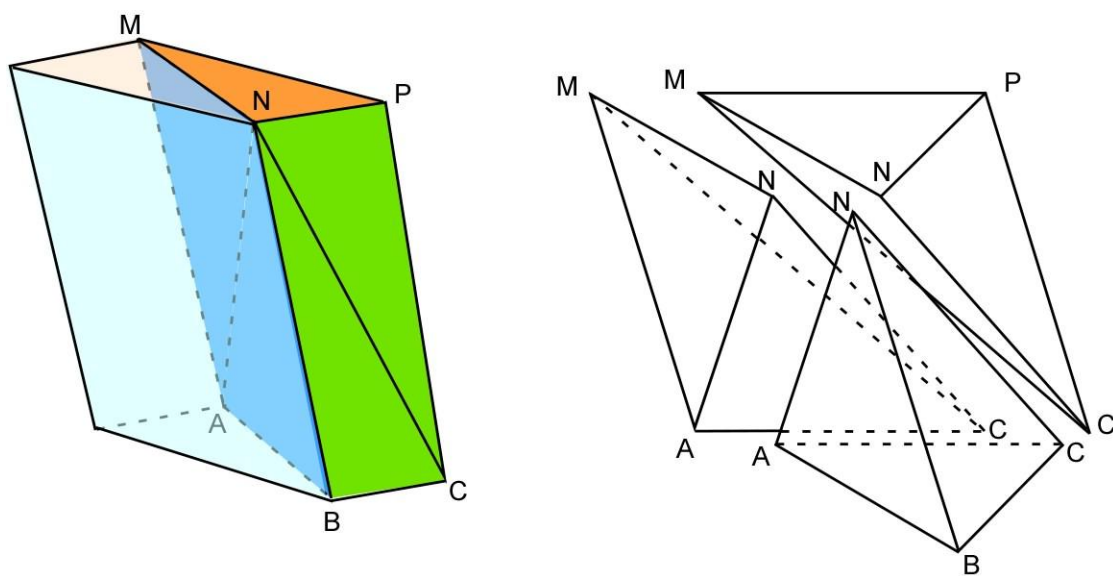


Fig. 8

**Fig. 9**

ACCEPTED MAN

**Fig. 10**

ACCEPTED MANUSCRIPT

Table 1

Site	Pos	N	n	Dec BAC	Inc BAC	$\alpha_{95}$	k	Str S0	Dip S0	Dec ABC	Inc ABC	$\alpha_{95}$	k
BG01	NW	16	14	241	-18	15	6	284	54	204	-48	15	7
BG02	NW	17	16	254	-10	11	13	285	57	228	-53	11	12
DA01	NW	63	63	249	-20	5	15	290	40	228	-45	5	15
RAD1	SW		19	26	36	12	8	160	23	6	50	13	7
SI02	SE	27	14	24	57	8	29	294	26	24	31	6	47
SI04	SE	36	6	21	59	10	25	341	28	41	36	5	223
SI05	SE	29	18	22	50	8	35	325	26	38	32	6	32
SS01	NE	10	7	170	-50	12	33	97	40	216	-45	11	33
SS02	NE	11	5	146	-33	8	104	102	81	235	-41	9	86
SS03	NE	12	11	192	-63	6	58	103	51	249	-34	7	54
SS04	NE	11	11	208	-73	5	114	95	43	253	-38	5	97
SS05	NE	21	7	227	-61	10	14	89	36	247	-31	10	14
SS06	NE	17	17	207	-59	6	35	82	41	234	-27	6	35
VV01	SW	19	18	231	-31	10	12	192	21	218	-43	10	12
VV02	SW	12	12	209	-27	4	49	188	24	198	-27	4	49

**Highlights**

1. The precise knowledge of a structure before and after deformation allows calculating deformation tensors.
2. The CT scanning of an analogue model with a reference system provides this knowledge.
3. A particular example shows this potentiality to understand complexly folded lineations and expected deformation patterns.

ACCEPTED MANUSCRIPT